A Dual-Broadband Dual-Polarized Directional Antenna for All-Spectrum Access Base Station Applications

Yejun He, *Senior Member, IEEE*, Yadong Yue, *Member, IEEE*, Long Zhang, *Member, IEEE*, and Zhi Ning Chen, *Fellow, IEEE*

***Abstract*— A dual-broadband, dual-polarized directional antenna with an electrical down-tilted beam is designed for all-spectrum access base station applications. Three columns of elements are deployed in the manner that six lower-band elements are placed in the center column while the eleven upper-band elements are arranged in the other two columns. Moreover, each column of elements are fed by two ports, which makes the proposed antenna suitable for multiple-input–multiple-output (MIMO) applications. To verify the design concept, a prototype is fabricated and measured. The measurement results confirm that the proposed antenna achieves a bandwidth of 31.6% (698–960 MHz) for VSWR<1.5 in the lower band and a bandwidth of 44.5% (1710–2690 MHz) for VSWR<1.5 in the upper band, covering all the frequency bands for 2G/3G/LTE systems and 700 MHz/2.6 GHz frequency bands. The measured gains are 17.4 ± 0.9 dBi, 17.3 ± 0.8 dBi, and 14.4 ± 0.9 dBi for the antenna port1, port2, and port3, respectively, while the third-order passive intermodulation (PIM_3) is larger than 115 dBm at all frequencies. With these distinctive advantages, the proposed antenna is suitable for multi-band base stations.**

***Index Terms*— All-spectrum access, base station antenna, directional antenna, dual-broadband, dual-polarized.**

I. Introduction

THE past two decades have witnessed the emergence of numerous communication systems operating at different frequencies. In China, the 2G communication systems, such as GSM900/GSM1800, CDMA, operate in the 900 MHz (825–960 MHz) and 1800 MHz (1710–1920 MHz) bands [1], while the 3G communication systems, such as TD-SCDMA, WCDMA, and CDMA2000, operate in the 2 GHz (1880–2170 MHz) band [2]. The LTE (4G) systems operate in the 2.3 GHz (2300–2400 MHz) and 2.6 GHz (2570–2690 MHz) bands [3], and it is expected that the 700 MHz (698–806 MHz) band will be applied to the 5G system (China Broadcasting Network Corporation Ltd.). In [4], a broadband ±45° dual-polarized base station antenna was proposed for 2G/3G/LTE bands, which operated from 1.7 to 2.7 GHz, but it was unable to cover the bands of LTE700, CDMA, and GSM 900. Therefore, it is challenging and advantageous to design a base station antenna that can cover GSM900/1800, TD-SCDMA, WCDMA, CDMA2000, and LTE700/2300/2600 bands as well as 700 MHz/2.6 GHz bands simultaneously.

Numerous research efforts were reported to meet the bandwidth coverage requirements, including multi-band, dual-band or dual-broadband designs [5]–[7]. Unfortunately, they were not ±45° slant dual-polarized or could not operate in the LTE700 MHz. In [5], a novel multiband vertical/horizontal polarized omnidirectional antenna was proposed for 2G/3G/LTE mobile communication systems, which achieved a bandwidth of 17.4% (806–960 MHz) and 35% (1880–2700 MHz), and a gain of 1.5 dBi and 4.5 dBi for vertical polarization (VP) and horizontal polarization (HP), respectively. A novel dual-band unidirectional antenna was presented in [6], and it operated from 0.78 to 1.1 GHz and from 1.58 to 2.62 GHz. However, this dual-band unidirectional antenna is difficult to implement in practical due to its large lateral dimension. In [7], a novel dual-broadband planar antenna element and array were proposed for 2G/3G/LTE mobile communications, which achieved a bandwidth of 22% (780–980 MHz) and 68% (1470–3000 MHz). To combat multipath fading and increase capacity [8], dual-polarized antennas, especially the ±45° slant polarized antennas were widely deployed.

Therefore, the antennas with advantages of dual-band and dual-polarized (DBDP) characteristics have attracted a great amount of interest in the base station area [9]–[14]. A novel dual-band broadband antenna array with dual polarization was proposed in [9], whose impedance bandwidths for the lower band and upper band only covered 806–960 and 1710–2170 MHz, respectively. Another DBDP microstrip antenna with a similar radiation pattern proposed in [11] had an impedance bandwidth of 17% (810–960 MHz), and 28% (1690–2240 MHz) in the lower

Manuscript received February 20, 2020; revised August 17, 2020; accepted August 20, 2020. Date of publication October 1, 2020; date of current version April 7, 2021. This work was supported in part by the National Natural Science Foundation of China under Grant 62071306 and Grant 61801299; in part by the Mobility Program for Taiwan Young Scientists under Grant RW2019TW001; and in part by the Shenzhen Science and Technology Program under Grant GJHZ 20180418190529516 and Grant JSGG 20180507183215520. *(Corresponding author: Yejun He)*

Yejun He, Yadong Yue, and Long Zhang are with the College of Electronics and Information Engineering, Shenzhen University, Shenzhen 518060, China (e-mail: heyejun@126.com; 765984073@qq.com; longzhang717@163.com).

Zhi Ning Chen is with the Department of Electrical and Computer Engineering, National University of Singapore, Singapore 117583 (e-mail: eleczn@nus.edu.sg).

Color versions of one or more of the figures in this article are available online at https://ieeexplore.ieee.org.

Digital Object Identifier 10.1109/TAP.2020.3026919

band and upper band, respectively. Nonetheless, it was unable to operate in LTE700/LTE2300/LTE2600 bands. Apart from the above antennas, a compact multiband and dual-polarized mobile base-station antenna using an optimal array structure was introduced in [15], which is unable to run in LTE700/LTE2600 bands as well.

The PCB technique was commonly applied to fabricate base station antennas [4], [7], [10], and [11], which inevitably resulted in unavoidable energy loss and high passive intermodulation. To alleviate these issues, metallic antennas made by metal stamping or casting processes can be used. Besides, multiple-input–multiple-output (MIMO) techniques have merged as one of the key technologies for the next generation mobile communication systems because they make it possible to achieve high spectrum efficiency and huge capacity without sacrificing additional frequency spectrum and transmitted power [16].

In this article, a novel dual-broadband, dual-polarized directional antenna with six ports and an electrical downtilt range of 0°–10° is proposed to simultaneously cover GSM900/GSM1800, TD-SCDMA, WCDMA, and CDMA2000, LTE700/LTE2300/LTE2600. Thus, the proposed antenna can greatly reduce repetitive construction costs of communication systems and related infrastructure. Moreover, the third-order passive intermodulation (PIM_3) of the proposed antenna is measured and analyzed in detail.

This article is organized as follows. Section II presents the antenna design and its structure. Section III gives necessary parametric studies and corresponding discussions. The measured results of the proposed antenna array are described in Section IV. Finally, conclusion is drawn in Section V.

II. Antenna Design and Configuration

To make a better description of the proposed antenna, we define the XOZ-plane as the horizontal plane (H-plane) and YOZ-plane as the vertical plane (V-plane). For base station applications in cellular mobile communication systems, antennas need to have a high gain, a narrow beamwidth in V-plane, a stable radiation pattern at H-plane, an adjustable downtilt beam and very low passive intermodulation. To increase the antenna gain and narrow the antenna beamwidth at V-plane, an antenna array is required. The topology of the proposed dual-broadband and dual-polarized antenna array is illustrated in Fig. 1.

The proposed antenna array is composed of low-frequency antenna elements, high-frequency antenna elements, the director patches right above each high-frequency antenna elements, isolation baffles, and a baffle-board. The low-frequency antenna element [17] looks like an octagonal bowl. Each low-frequency antenna element consists of a bowl-shaped base bottom, four couples of baluns and two pairs of dipoles that are orthogonal to each other to form ±45° polarization. The low-frequency elements operate in a bandwidth of 31.6% (0.698–0.96 MHz). It not only operates for LTE700/CDMA/GSM900, but also features good electrical performance and stable radiation patterns, which are easily applied to form a dual-band base station antenna

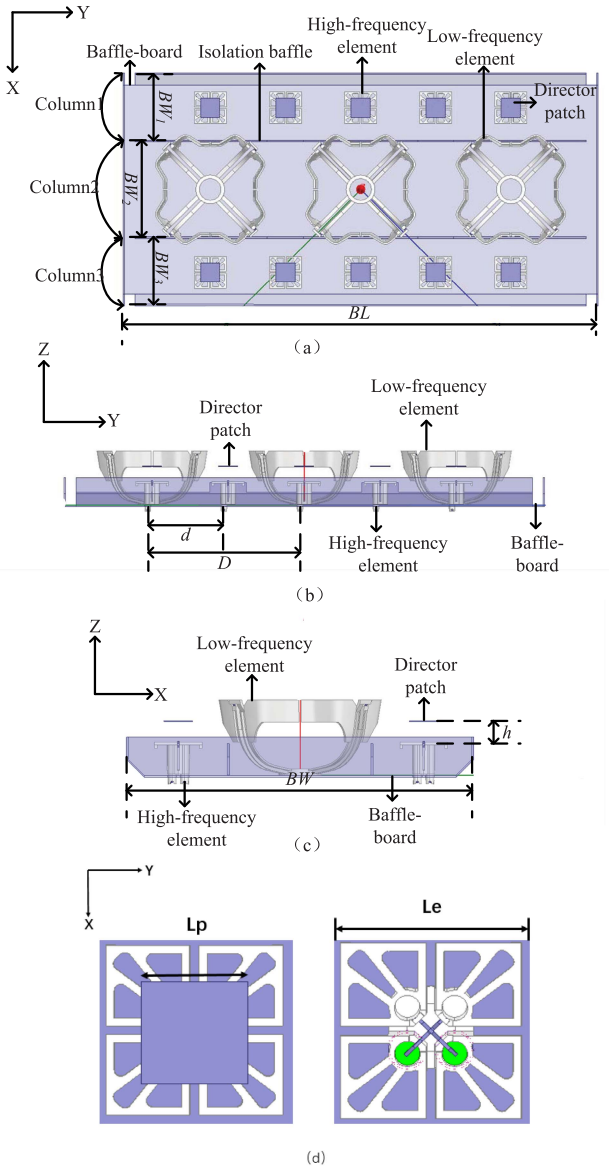

Fig. 1. Geometry of the proposed antenna. (a) Top view. (b) Front view. (c) Side view. (d) Zoomed view of high-frequency antenna element.

arrays together with high frequency antenna elements. The high-frequency element mainly consists of two pairs of square-loop dipoles orthogonal to each other, a pair of feed bars and two pairs of baluns. Based on the square-loop radiator dipoles, the high-frequency antenna element [18] is developed with two pairs of parasitic metal stubs and four pairs of parasitic metal branches to obtain wider impedance bandwidths. The high-frequency elements can cover the bandwidth of 44.5% (1710–2690 MHz) for VSWR < 1.5. In addition, the high-frequency antenna element features broadband dual-polarized characteristics. By combining the broadband dual-polarized low-frequency radiation element and the broadband dual-polarized high-frequency antenna element, a dual-broadband and dual-polarized antenna is obtained. The introduction of baffle-board is to get directional radiation pattern. Since the antenna gain is proportional to the number of elements [19], we introduce six low-frequency radiation elements to obtain a gain of 15 dBi in the middle column

TABLE I
COMPARISON BETWEEN VARIOUS LOW-FREQUENCY ANTENNA ELEMENTS USED IN THIS WORK AND OTHER WORKS

Ref	Antenna Type	Bandwidth	Size (mm^3)	Peak Gain (dBi)
[11]	Microstrip antenna	16.94%(810-960 MHz)	$0.71\lambda_0$*$0.71\lambda_0$*$0.11\lambda_0$	9.4
[10]	Patch Antenna	20.45%(790-970 MHz)	$0.76\lambda_0$*$0.79\lambda_0$*$0.34\lambda_0$	10.2
[7]	Metallic dipole	20.22%(800-980 MHz)	$0.46\lambda_0$*$0.38\lambda_0$*$0.13\lambda_0$	9.0
[25]	Metallic dipole	32.7% (690-960 MHz)	$0.46\lambda_0$*$0.46\lambda_0$*$0.12\lambda_0$	9.4
This work	Metallic dipole	31.6%(698-960 MHz)	$0.46\lambda_0$*$0.46\lambda_0$*$0.23\lambda_0$	9.9

(column 2), and eleven high-frequency antenna elements to get a composite gain of 18 dBi for the other two columns (columns 1 and 3). Besides, there are two ports connecting to each column of elements. For simplicity, we just choose three low-frequency antenna elements in the middle column and five high-frequency antenna elements in the outer two columns to conduct simulation.

We have made a comparison between several low-frequency antenna elements used in this work and other works. The result is listed in Table I. The proposed antenna performs well in gain, bandwidth, and size. Although study as mentioned in [25] can achieve wider bandwidth and smaller size than that of the low-frequency antenna element proposed in this article, the VSWR quantified in [25] is less than 2 instead of less than 1.5.

The simulated model of the proposed phase shifter working in lower band is shown in Fig. 2, which consists of a shell, two dielectric plates, and two conductor lines printed on the substrate (dielectric constant = 2.5) to form a feed network. As the working mechanism and implementation of phase shifter has been carried out in [22], we only briefly describe the structure and feed circuits of two phase shifters. The power distribution on the port is realized by the width of the conductor line in feed network. The dielectric plate is designed to guarantee the VSWR and power distribution ratio, and sufficient phase change can also be obtained to meet the requirements of the downtilt angle of the proposed antenna array. The phase difference is achieved by moving the position of the dielectric plate to change the permittivity of the transmission path. P1 is the input port, and P2, P3, P4, P5, and P6 are the output ports. Note that since the phase shifter has only five output ports, the last two lower band elements shown in Fig. 3(a) connect to P6, and the phase difference between the last two lower band elements is achieved by cable. The phase shifter working in upper band is similar to the phase shifter working in lower band, with eleven output ports instead of five output ports.

As depicted in Fig. 3, the left feeding circuit and right one are designed for the lower frequency band and upper frequency band, respectively. They mainly consist of some power dividers, some low loss transmission devices and several coaxial cables. When the bar of the antenna is pulled a certain scale, the phase of every element in the same column changes correspondingly. In addition, the $\triangle$ stands for a phase increment. When the phase of the middle element is set to zero, phases of other elements are shown in Fig. 3. The mechanism

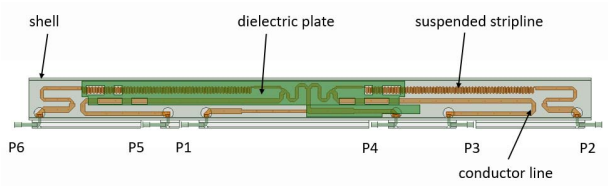

Fig. 2. Simulated model of lower-band phase shifter.

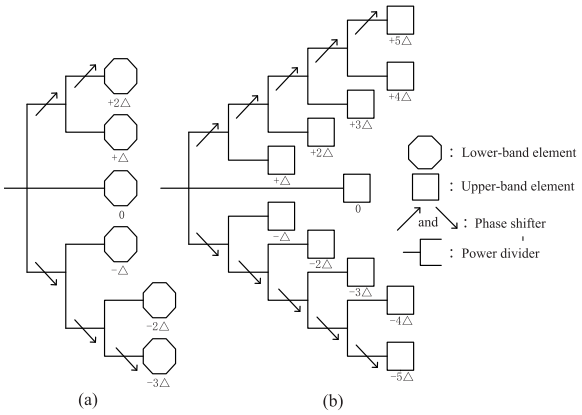

Fig. 3. Feed circuits of two phase shifters. (a) Feed circuit of lower-band phase shifter. (b) Feed circuit of upper-band phase shifter.

is that the phase displacement is generated by changing the permittivity of the transmission medium.

III. PARAMETRIC STUDY AND DISCUSSION

In the process of simulation optimization, many factors have been taken into account, including the length, height and width of the baffle-board, the location of the isolation baffle and the dimensions of the director patch. We make a detailed discussion with respect to two key factors, the spacing between adjacent elements and the height of the director patches, which is given as follows.

A. Spacing

The foremost parameter of the proposed antenna is the spacing between adjacent elements. For a better description of the spacing between adjacent elements, we use a letter d standing for the spacing between adjacent high-frequency radiation elements, and D standing for the spacing between adjacent low-frequency radiation elements. It is worth mentioning that when we studied the effects of spacing between

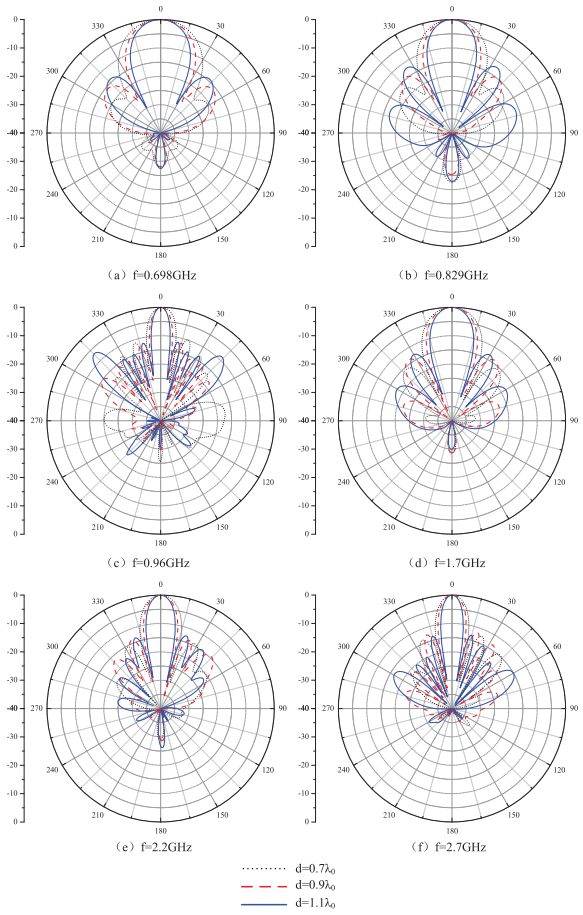

Fig. 4. Effects of spacing between adjacent high-frequency radiation elements on V-plane of the antenna.

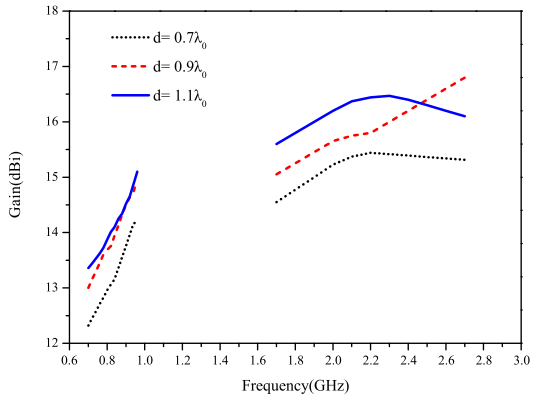

Fig. 5. Effects of spacing between adjacent high-frequency radiation elements on the gain of the antenna.

high-frequency elements, we moved high-frequency elements and low-frequency elements together to prevent the effects brought by the change of the relative position between high-frequency elements and low-frequency elements. Simulated V-plane radiation patterns for different spacings between adjacent high-frequency radiation elements at 0.698, 0.829, 0.96, 1.7, 2.2, and 2.7 GHz are, respectively, shown in Fig. 4, where λ_0 is the free-space wavelength at the center frequency (2.2 GHz) of the upper band. From Fig. 4, it can be seen that the V-plane beam decreases with the increase of element spacing. However, when the array element spacing is larger

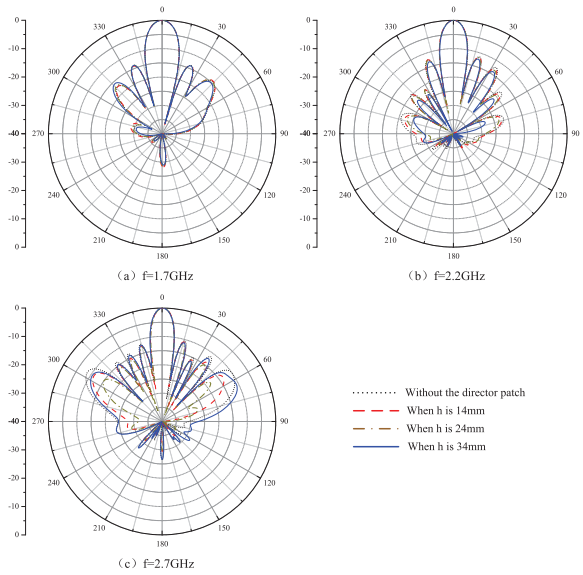

Fig. 6. Effects of the height of the director patch on V-plane of the antenna.

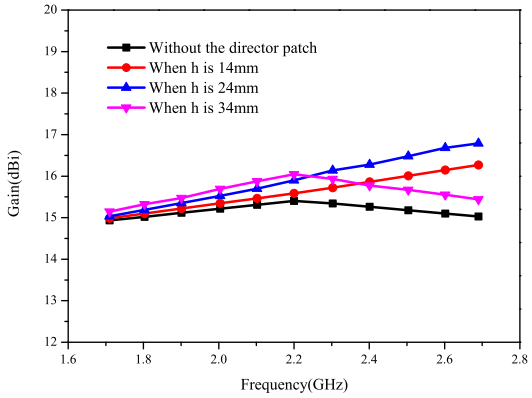

Fig. 7. Effects of the height of the director patch on the gain of the antenna.

than $0.9\lambda_0$, high sidelobe occurs, including the appearance of a grating lobe at 2.7 GHz. Additionally, the larger the array element spacing, the greater the antenna array gain shown in Fig. 5. However, there is an exception for 2.7 GHz frequency point because the array element spacing is considerably longer than the wavelength at the 2.7 GHz, leading to the appearance of grating lobes and lower gain. Therefore, $0.9\lambda_0$ (125 mm) is an ideal choice after a tradeoff between the antenna array gain and the V-plane radiation patterns. For the high-frequency range from 1710 to 2690 MHz and the low-frequency range from 698 to 960 MHz, the high-frequency radiation element operating frequency is almost twice as much as the low-frequency radiation element operating frequency. The wavelength corresponding to high-frequency radiation element is around half of the wavelength corresponding to low-frequency element, therefore it is a reasonable choice that the spacing between the low-frequency radiation elements is 250 mm.

B. Height

As aforementioned, patch directors which are supported by plastic pillars above each high-frequency element, are used to

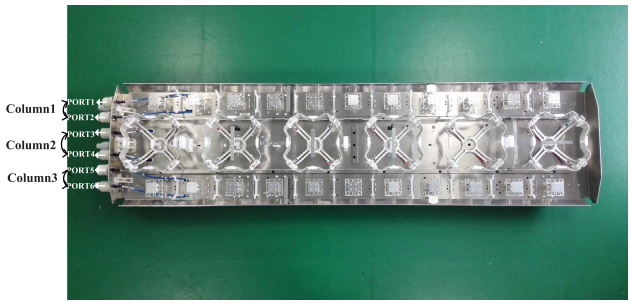

Fig. 8. Prototype of the proposed dual-broadband and dual-polarized antenna (front view).

TABLE II
OPTIMAL DIMENSIONS OF THE PROPOSED ANTENNA

Parameter	Value(mm)	Parameter	Value(mm)
d	125	h	24
D	250	BW_1	110
BL	750	BW_2	160
BW	380	BW_3	110
Le	53	Lp	32

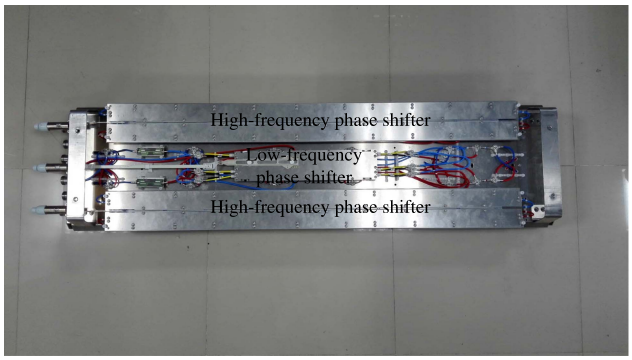

Fig. 9. Phase shifter on the back view of the proposed dual-broadband and dual-polarized antenna prototype.

improve the antenna gain. As depicted in Fig. 6, it can be easily observed that the V-plane radiation pattern at 1.7 and 2.2 GHz remains almost the same as that without the director patch while the V-plane radiation pattern at 2.7 GHz changes significantly with the increase of h. In addition, as shown in Fig. 7, the antenna array gain increases as h increases from 1.7 to 2.2 GHz. However, when h is 34 mm, the antenna array gain at 2.7 GHz decreases drastically due to the appearance of a high grating lobe. Thus, 24 mm is chosen to obtain a stable V-plane radiation pattern and the antenna array gain.

IV. RESULTS

In order to verify the design, a proof-of-concept prototype of the proposed dual-broadband and dual-polarized antenna array is fabricated, as illustrated in Fig. 8. Additionally, in order to obtain an adjustable downtilt of the antenna beam, a low-frequency phase shifter and two high-frequency phase shifters are introduced as shown in Fig. 9. Compared with the mechanical downtilt, electrical downtilt has the distinctive advantage of a more stable radiation pattern in H-plane and features no significant adjacent interference when the degree of downtilt is changed greatly. The optimal dimensions of the proposed dual-broadband and dual-polarized antenna array are tabulated in Table II.

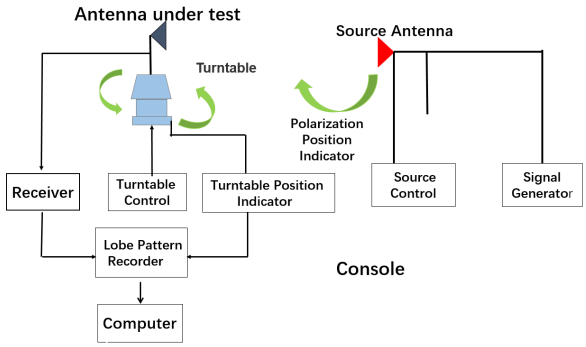

Fig. 10. Basic structure of the test system in the anechoic chamber.

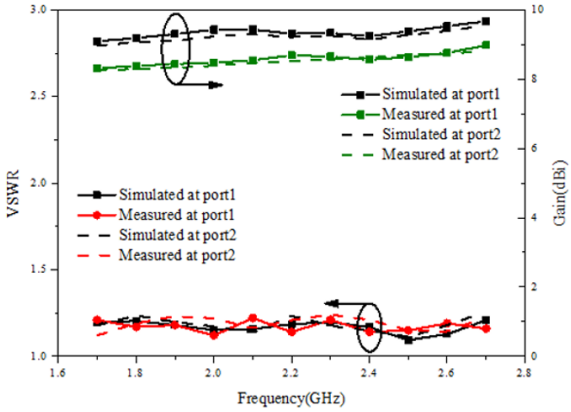

Fig. 11. Simulated and measured VSWR and gains of high-frequency element.

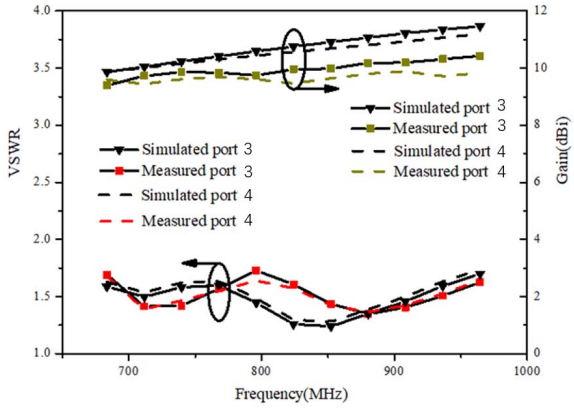

Fig. 12. Simulated and measured VSWR and gains of low-frequency element.

The performance of the proposed antenna is simulated in HFSS 16.1. The electrical performance is measured by Agilent E5061B network analyzer in an anechoic chamber and the radiation performance is tested by a far-field testing system. Fig. 10 shows the basic structure of the test system in the anechoic chamber. The whole antenna measurement system includes the antenna under test (AUT), the source antenna, the turntable, the console and the computer. After the polarization position is confirmed, the signal generator sends the signal to the AUT through the source antenna. The AUT collects lobe pattern sampling values through rotating around its axis, and then the sampling values are sent to

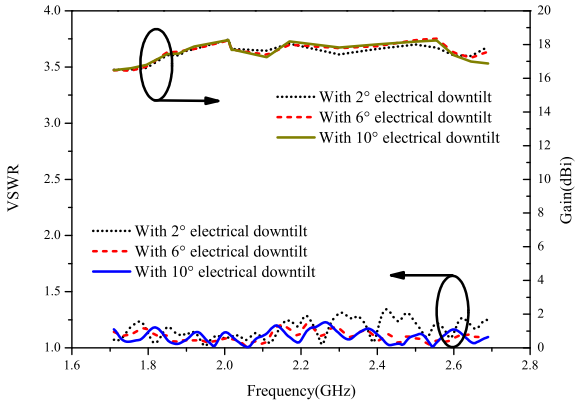

(a)

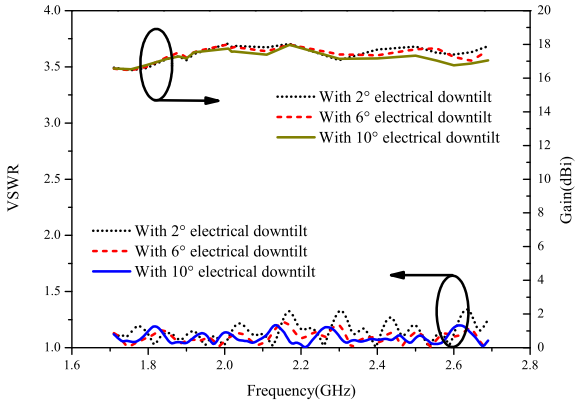

(b)

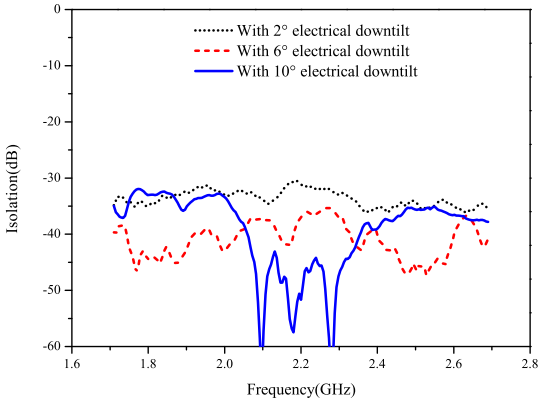

(c)

Fig. 13. (a) Measured VSWR and gain of the proposed antenna at port1 with 2°, 6°, and 10° of downtilt. (b) Measured VSWR and gain of the proposed antenna at port2 with 2°, 6°, and 10° of downtilt. (c) Measured isolation of the proposed antenna between port1 and port2 with 2°, 6°, and 10° of downtilt.

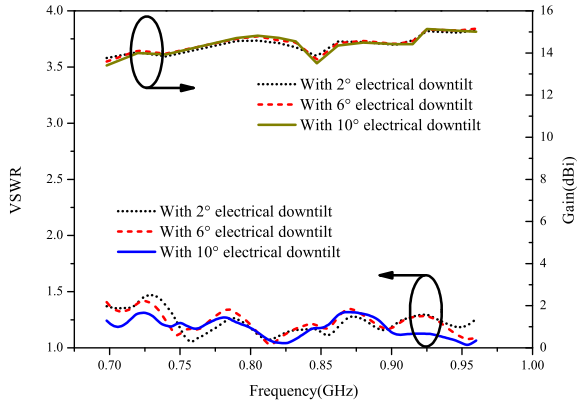

(a)

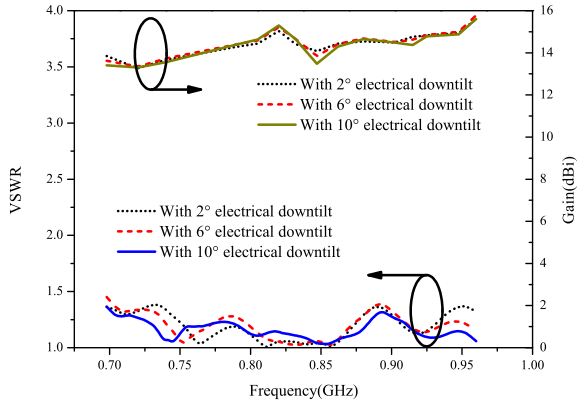

(b)

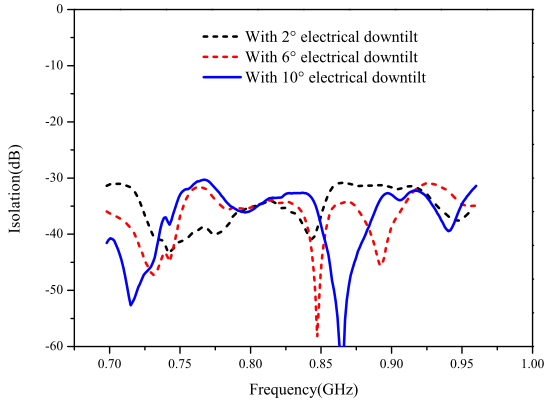

(c)

Fig. 14. (a) Measured VSWR and gain of the proposed antenna at port3 with 2°, 6°, and 10° of downtilt. (b) Measured VSWR and gain of the proposed antenna at port4 with 2°, 6°, and 10° of downtilt. (c) Measured isolation of the proposed antenna between port3 and port4 with 2°, 6°, and 10° of downtilt.

the lobe pattern recorder. Finally, the data are output to the computer for data processing. This test system can accurately measure the antenna radiation pattern, polarization, gain, and other parameters. It is almost fully automated, which can save measurement time and greatly improve the efficiency of antenna research and development.

Fig. 11 shows simulated and measured VSWR and gains of high-frequency element, and Fig. 12 shows simulated and measured VSWR and gains of low-frequency element. It can be seen that the VSWR simulated and measured for the two ports is lower than 1.5 in the upper operating frequency band (from 1.7 to 2.7 GHz) and lower than 1.7 in the lower

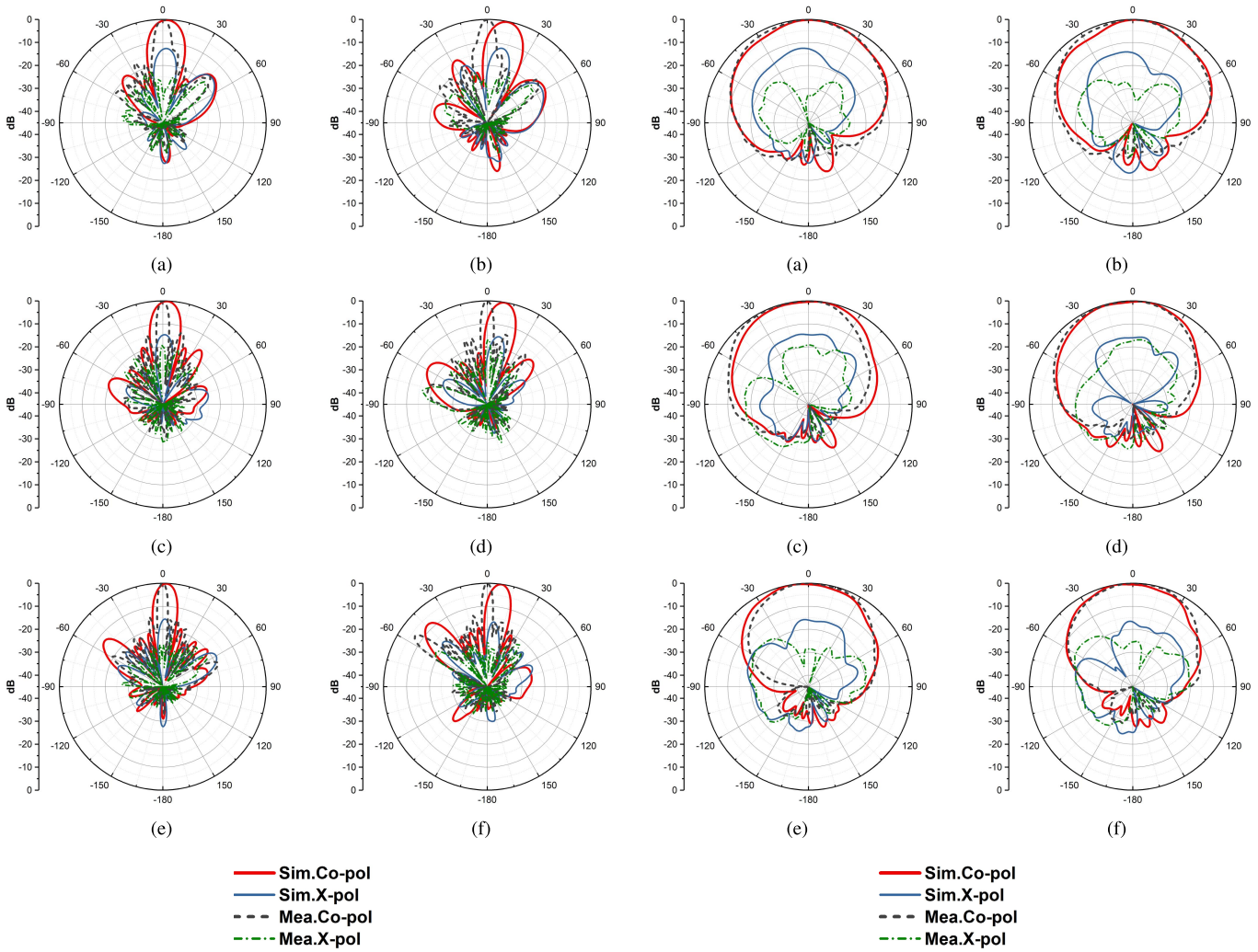

Fig. 15. Simulated and measured V-plane radiation patterns of the proposed antenna excited at Port 1 (ED denotes electrical downtilt). (a) f = 1.7 GHz (ED = 2°). (b) f = 1.7 GHz (ED = 10°). (c) f = 2.2 GHz (ED = 2°). (d) f = 2.2 GHz (ED = 10°). (e) f = 2.7 GHz (ED = 2°). (f) f = 2.7 GHz (ED = 10°).

Fig. 16. Simulated and measured H-plane radiation patterns of the proposed antenna excited at Port 1 (ED denotes electrical downtilt). (a) f = 1.7 GHz (ED = 2°). (b) f = 1.7 GHz (ED = 10°). (c) f = 2.2 GHz (ED = 2°). (d) f = 2.2 GHz (ED = 10°). (e) f = 2.7 GHz (ED = 2°). (f) f = 2.7 GHz (ED = 10°).

operating frequency band (from 698 to 960 MHz), respectively. The simulated VSWR results are in good agreement with the measured ones. As can be seen, the simulated and measured gains of the lower band are about 10 and 9.5 dBi, respectively, while the gains of the upper band are about 9.3 and 8.5 dBi. Although the simulated gains are better than the measured gains, the two results are stable in the whole frequency band. The difference between the simulated and measured results may be resulted from the insertion loss introduced in the connection between the coaxial cables and SMA connectors.

From Figs. 13(a) and (b) and 14(a) and (b), we can easily observe that the measured VSWRs at port1, port2 and port3, port4 with 2°, 6°, and 10° of downtilt are less than 1.5 from 1.7 to 2.7 GHz and from 0.698 to 0.96 GHz, respectively. The measured gains with 2°, 6°, and 10° of downtilt at port1, port2 and port3, port4 are about 17.4, 17.3 dBi and 14.4 and 14.5 dBi, respectively. Moreover, the VSWRs and gain values remain almost stable as the degree of the downtilt of the proposed antenna array is increased. Nevertheless, Figs. 13(c) and 14(c) show that as the degree of the downtilt of the proposed antenna array increases, the measured isolation values between port1, port2 and port3, port4 change dramatically, which remain better than 29 dB over the whole desired bands and meet the basic electrical specifications of base station antennas.

Since the radiation patterns are symmetric between port1&6, port2&5, and port3&4, the simulated and measured radiation patterns of the antenna array with 2° and 10° of downtilt at frequency of 1.7, 2.2, and 2.7 GHz at port1, 1.7, 2.2, and 2.7 GHz at port2 and 0.698, 0.829, and 0.96 GHz at port3 are shown in Figs. 15–20, respectively.

Good agreement between simulation results and measurement results can be observed. For simplicity, we just choose three low-frequency radiation elements in the middle column and five high-frequency radiation elements in the outer two columns to conduct simulation. In practical measurement, we use six low-frequency radiation elements in the middle column and eleven high-frequency radiation elements in the outer two columns. Thus, there are huge differences between

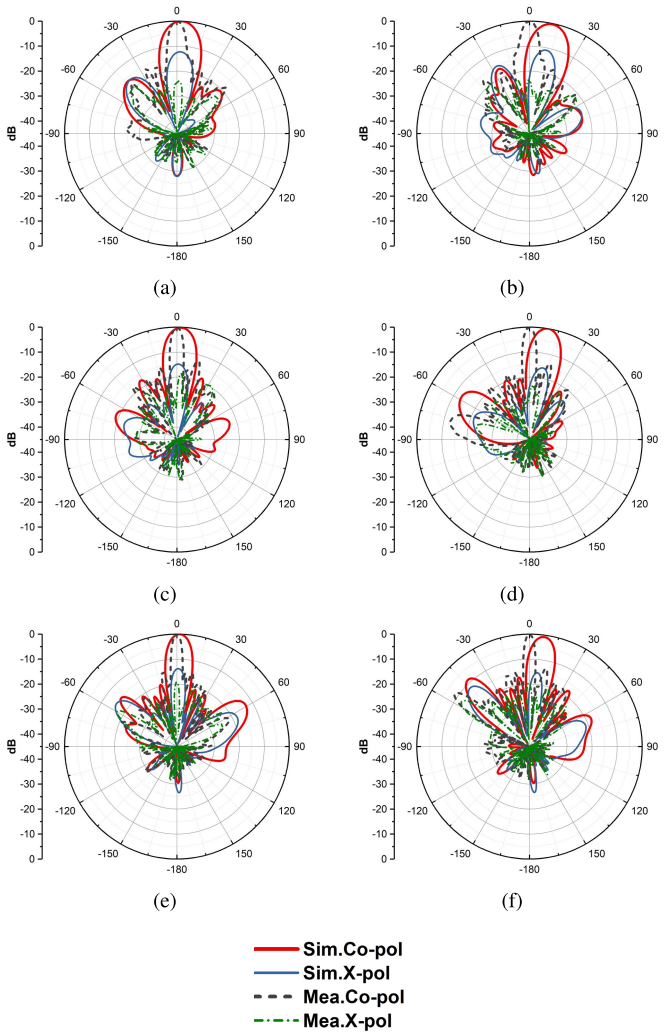

Fig. 17. Simulated and measured V-plane radiation patterns of the proposed antenna excited at Port 2 (ED denotes electrical downtilt). (a) f = 1.7 GHz (ED = 2°). (b) f = 1.7 GHz (ED = 10°). (c) f = 2.2 GHz (ED = 2°). (d) f = 2.2 GHz (ED = 10°). (e) f = 2.7 GHz (ED = 2°). (f) f = 2.7 GHz (ED = 10°).

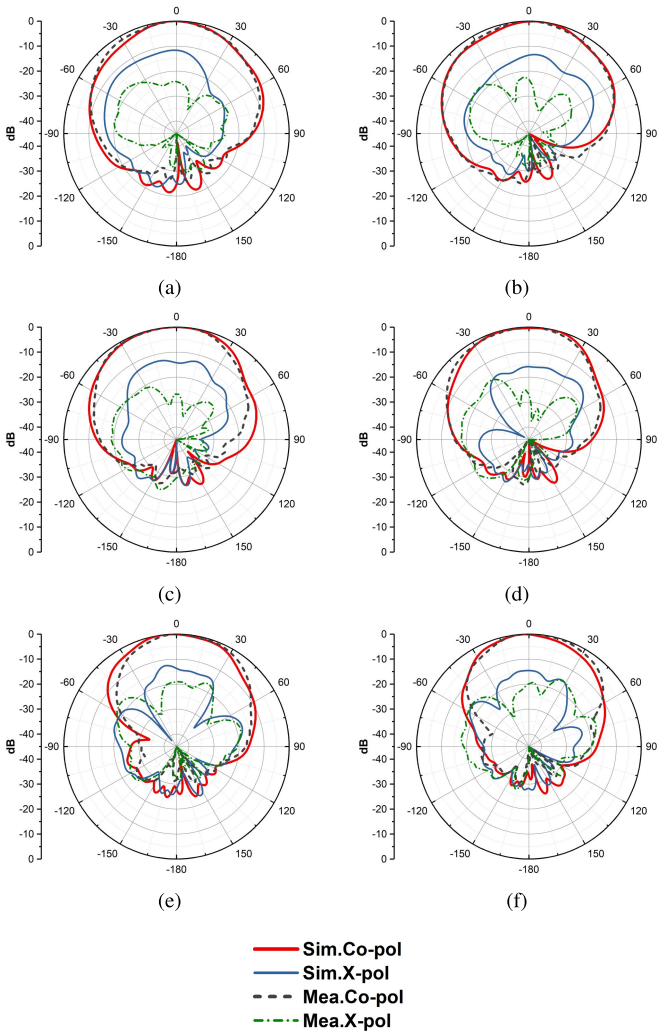

Fig. 18. Simulated and measured H-plane radiation patterns of the proposed antenna excited at Port 2 (ED denotes electrical downtilt). (a) f = 1.7 GHz (ED = 2°). (b) f = 1.7 GHz (ED = 10°). (c) f = 2.2 GHz (ED = 2°). (d) f = 2.2 GHz (ED = 10°). (e) f = 2.7 GHz (ED = 2°). (f) f = 2.7 GHz (ED = 10°).

the simulated and measured radiation patterns in Figs. 15, 17, and 19. It is also shown that stable radiation patterns, low first upper sidelobe level and good downtilted performance are achieved at V-plane over all operating bands. Since the two columns of high-frequency radiation elements are not situated on the center of the baffle-board, the H-plane radiation patterns are slightly affected. The differences between the simulated and measured X-pol levels may be caused by insufficient machine accuracy and fabrication measurement errors. In addition, it is worth mentioning that the influence of grating lobes at 2.2 and 2.7 GHz is negligible because the grating lobes are out of illuminated coverage of the proposed antenna array.

The PIM_3 has become an important specification for base station antennas in cellular communication systems, which is tested by Kaelus PIM test analyzers as shown in Fig. 21. As shown in Fig. 22, all of the PIM_3 with downtilt of 2° and 10° at frequencies of 700, 900, 1800, 2100, and 2600 MHz are more than 115 dBm, which is much better than the PIM_3 requirement of 107 dBm using two 20 W (2*43 dBm) carriers for industrial manufacture. And we find that the PIM_3 with 10° of downtilt is better than that with 2° of downtilt. It is concluded that the low PIM_3 is owing to following four factors: 1) both the high-frequency elements and the low-frequency elements are fabricated by using the die-casting technique and then electroplated with nickel and tin, which makes the antenna elements better connected with the coaxial cables. This changes the superficial skin depth of its plating and reduces its nonlinearity as well; 2) a plastic slice is mounted on each hole of the baffle-board to avoid the direct contact between the element and the baffle-board; 3) each port of the proposed antenna array is wiped by industrial alcohol and every operator wears a pair of gloves during the assembling process, which ensures the proposed antenna array suffers from minimum contamination; and 4) the proposed antenna array is packed into a fiberglass, sealed by a special glue. The rain test is also conducted in order to check its leakproofness. Otherwise, the ferromagnetic material will form easily and affect PIM_3 performance [20].

TABLE III
COMPARISON OF VARIOUS ANTENNAS

Ref	Bandwidth	Isolation	HPBW	Gain	Array
[17]	31.6%(0.698-0.96 GHz)	>25 dB	65.92°±5.44°	~9.5 dBi	NA
[18]	45.5%(1.7-2.7 GHz)	>30 dB	65.2°±5.6°	8.5±0.4 dBi	NA
[21]	19.4%(0.79-0.96 GHz)	>28 dB	65°±5°	~15.1 dBi	5 elements
	23.7%(1.71-2.17 GHz)	>28 dB	65.2°±5.6°	~17.3 dBi	10 elements
[22]	44.5%(1.71-2.69 GHz)	>31 dB	65°±5°	15 ±1.1 dBi	6 elements
[23]	45.5%(1.7-2.7 GHz)	>28 dB	64.85°±4.12°	>14.23 dBi	10 elements
[24]	46.9%(1.55-2.5 GHz)	>35 dB	NG	~13.5 dBi	4 elements
This work	31.6%(0.698-0.96 GHz)	>29 dB	66°±5.3°	~14.4 dBi	6 elements
	44.5%(1.71-2.69 GHz)	>29 dB	65°±5.2°	~17.3 dBi	11 elements

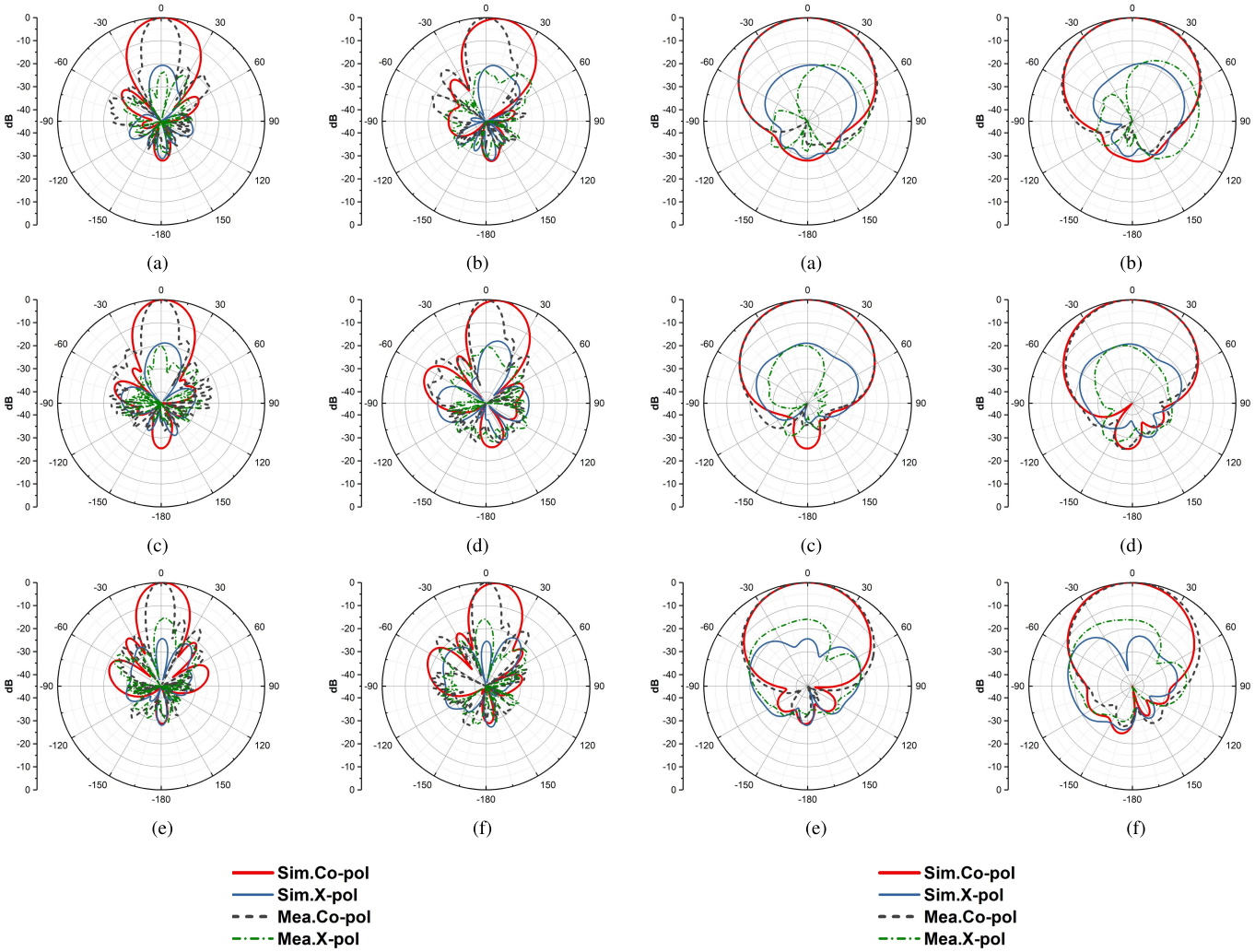

Fig. 19. Simulated and measured V-plane radiation patterns of the proposed antenna excited at Port 3 (ED denotes electrical downtilt) (a) f = 0.698 GHz (ED = 2°). (b) f = 0.698 GHz (ED = 10°). (c) f = 0.829 GHz (ED = 2°). (d) f = 0.829 GHz (ED = 10°). (e) f = 0.96 GHz (ED = 2°). (f) f = 0.96 GHz (ED = 10°).

Fig. 20. Simulated and measured H-plane radiation patterns of the proposed antenna excited at Port 3 (ED denotes electrical downtilt) (a) f = 0.698 GHz (ED = 2°). (b) f = 0.698 GHz (ED = 10°). (c) f = 0.829 GHz (ED = 2°). (d) f = 0.829 GHz (ED = 10°). (e) f = 0.96 GHz (ED = 2°). (f) f = 0.96 GHz (ED = 10°).

The comparison of the proposed array with some earlier reported base station antennas in terms of the bandwidth, HPBW, gain, etc., is carried out and summarized in Table III. He *et al.* [17] and He and Yue [18] only designed antenna elements to work in a single band, which is 0.698–0.98 and 1.7–2.7 GHz, respectively. He *et al.* [22], Zheng and Chu [23], and Lian *et al.* [24] have designed antenna arrays, but they can only cover a single band. Though He *et al.* [21] designed

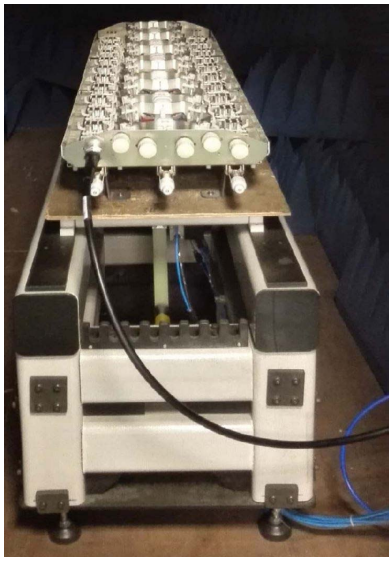

Fig. 21. Proposed antenna is tested on PIM_3.

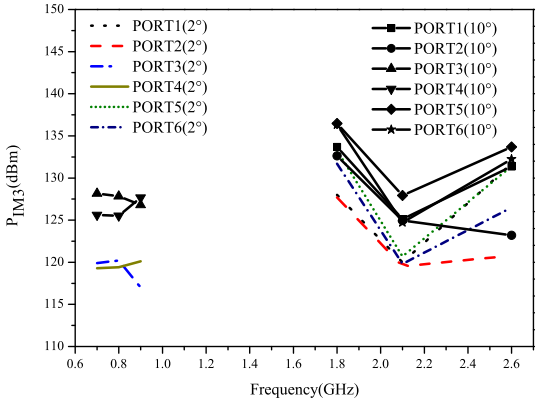

Fig. 22. PIM_3 of the proposed antenna with 2° and 10° of downtilt at different frequencies.

an antenna array that covers dual band and achieves better gain, the antenna array proposed by us has a wider operating bandwidth and better isolation.

V. Conclusion

A dual-broadband, dual-polarized directional antenna with an electrical downtilt range of 0°–10° is proposed. It can support the all-spectrum access communication applications covering GSM900/GSM1800, TD-SCDMA, WCDMA, and CDMA2000, LTE700/LTE2300/LTE2600 as well as 700 MHz/2.6 GHz frequency bands simultaneously. Measured results indicate that the proposed antenna array achieves wide impedance bandwidths of 31.6% (698–960 MHz) in the lower band and 44.5% (1710–2690 MHz) in the upper band, respectively. Compared with other reported DBDP antennas, the proposed antenna features wider impedance bandwidth, better downtilted performance and much lower PIM_3. Due to these advantages, the proposed antenna is promising for applications in sub-6 GHz base stations.

References

[1] P. Nicopolitidis, M. S. Obaidat, G. I. Papadimitriou, and A. S. Pomportsis, *Wireless Networks*. New York, NY, USA: Wiley, 2003.

[2] G. Liu, J. Zhang, P. Zhang, Y. Wang, X. Liu, and S. Li, "Evolution map from TD-SCDMA to FuTURE B3G TDD," *IEEE Commun. Mag.*, vol. 44, no. 3, pp. 54–61, Mar. 2006.

[3] *ITU-R Resolution [COM5/24] to WRC-2000*, ITU-R, Istanbul, Turkey, 2000. [Online]. Available: http://www.itu.int/newsarchive/wrc2000/IMT-2000/Res-COM5-24.html

[4] Q.-X. Chu, D.-L. Wen, and Y. Luo, "A broadband ±45° dual-polarized antenna with Y-Shaped feeding lines," *IEEE Trans. Antennas Propag.*, vol. 63, no. 2, pp. 483–490, Feb. 2015.

[5] X.-W. Dai, Z.-Y. Wang, C.-H. Liang, X. Chen, and L.-T. Wang, "Multi-band and dual-polarized omnidirectional antenna for 2G/3G/LTE application," *IEEE Antennas Wireless Propag. Lett.*, vol. 12, pp. 1492–1495, 2013.

[6] W. X. An, H. Wong, K. L. Lau, S. F. Li, and Q. Xue, "Design of broadband dual-band dipole for base station antenna," *IEEE Trans. Antennas Propag.*, vol. 60, no. 3, pp. 1592–1595, Mar. 2012.

[7] Y. Cui, R. Li, and P. Wang, "Novel dual-broadband planar antenna and its array for 2G/3G/LTE base stations," *IEEE Trans. Antennas Propag.*, vol. 61, no. 3, pp. 1132–1139, Mar. 2013.

[8] B. Lindmark and M. Nilsson, "On the available diversity gain from different dual-polarized antennas," *IEEE J. Sel. Areas Commun.*, vol. 19, no. 2, pp. 287–294, Feb. 2001.

[9] X. Liu, S. He, H. Zhou, J. Xie, and H. Wang, "A novel low-profile, dual-band, dual-polarization array antenna for 2G/3G base station," in *Proc. IET Int. Conf. Wireless Mobile Multimedia Netw. (ICWMMN)*, Nov. 2006, pp. 1–4.

[10] M. Kaboli, M. S. Abrishamian, S. A. Mirtaheri, and S. M. Aboutorab, "High-isolation XX-polar antenna," *IEEE Trans. Antennas Propag.*, vol. 60, no. 9, pp. 4046–4055, Sep. 2012.

[11] Y. Wang and Z. Du, "Dual-polarized dual-band microstrip antenna with similar-shaped radiation pattern," *IEEE Trans. Antennas Propag.*, vol. 63, no. 12, pp. 5923–5928, Dec. 2015.

[12] X. Zhang, G. Yang, X. Wang, and B. Li, "A dual-band and dual-polarized antenna array for 2G/3G/LTE base stations," *Int. J. RF Microw. Comput.-Aided Eng.*, vol. 26, no. 2, pp. 154–163, Feb. 2016.

[13] Z. Liu, J. Liu, Z. Liu, Y. Zhang, and X.-Y. Zhang, "A novel dual-band and high-gain antenna for 2G/3G base station," *Prog. Electromagn. Res. Lett.*, vol. 54, pp. 1–6, 2015.

[14] Y. He, Z. Pan, X. Cheng, Y. He, J. Qiao, and M. M. Tentzeris, "A novel dual-band, dual-polarized, miniaturized and low-profile base station antenna," *IEEE Trans. Antennas Propag.*, vol. 63, no. 12, pp. 5399–5408, Dec. 2015.

[15] Y.-B. Jung and S.-Y. Eom, "A compact MultiBand and dual-polarized mobile base-station antenna using optimal array structure," *Int. J. Antennas Propag.*, vol. 2015, pp. 1–11, 2015.

[16] M. A. Jensen and J. W. Wallace, "A review of antennas and propagation for MIMO wireless communications," *IEEE Trans. Antennas Propag.*, vol. 52, no. 11, pp. 2810–2824, Nov. 2004.

[17] Y. He, Y. Yue, and Z. Shen, "A novel broadband dual-polarized antenna element for LTE700 MHz/GSM850 MHz/GSM900 MHz applications," *IEEE Access*, vol. 4, pp. 4321–4326, 2016.

[18] Y. He and Y. Yue, "A novel broadband dual-polarized dipole antenna element for 2G/3G/LTE base stations," in *Proc. IEEE Int. Conf. RFID Technol. Appl. (RFID-TA)*, Sep. 2016, pp. 112–116.

[19] M. T. Ivrlac and J. A. Nossek, "Receive antenna gain of uniform linear arrays of isotrops," in *Proc. IEEE Int. Conf. Commun.*, Jun. 2009, pp. 1–6.

[20] J. J. Krstansky and R. F. Elsner, "Environment-generated intermodulation in communication complexes," in *Proc. 10th Tri-Service Conf. Electro-Magn. Compat.*, Nov. 1964, p. 77.

[21] Y. He, W. Tian, and L. Zhang, "A novel dual-broadband dual-polarized electrical downtilt base station antenna for 2G/3G applications," *IEEE Access*, vol. 5, pp. 15241–15249, 2017.

[22] Y. He, J. Li, S. W. Wong, X. Pan, L. Zhang, and Z. N. Chen, "A miniaturized base station antenna with novel phase shifter for 3G/LTE applications," *IEEE Access*, vol. 6, pp. 52877–52888, 2018.

[23] D.-Z. Zheng and Q.-X. Chu, "A wideband dual-polarized antenna with two independently controllable resonant modes and its array for base-station applications," *IEEE Antennas Wireless Propag. Lett.*, vol. 16, pp. 2014–2017, Jul. 2017.

[24] R. Lian, Z. Wang, Y. Yin, J. Wu, and X. Song, "Design of a low-profile dual-polarized stepped slot antenna array for base station," *IEEE Antennas Wireless Propag. Lett.*, vol. 15, pp. 362–365, 2016.

[25] Y. Chen, J. Zhao, and S. Yang, "A novel stacked antenna configuration and its applications in dual-band shared-aperture base station antenna array designs," *IEEE Trans. Antennas Propag.*, vol. 67, no. 12, pp. 7234–7241, Dec. 2019.

Yejun He (Senior Member, IEEE) received the Ph.D. degree in information and communication engineering from the Huazhong University of Science and Technology (HUST), Wuhan, China, in 2005.

From 2005 to 2006, he was a Research Associate with the Department of Electronic and Information Engineering, The Hong Kong Polytechnic University, Hong Kong. From 2006 to 2007, he was a Research Associate with the Department of Electronic Engineering, Faculty of Engineering, The Chinese University of Hong Kong, Hong Kong. In 2012, he was a Visiting Professor with the Department of Electrical and Computer Engineering, University of Waterloo, Waterloo, ON, Canada. From 2013 to 2015, he was an Advanced Visiting Scholar (Visiting Professor) with the School of Electrical and Computer Engineering, Georgia Institute of Technology, Atlanta, GA, USA. Since 2011, he has been a Full Professor with the College of Electronics and Information Engineering, Shenzhen University, Shenzhen, China, where he is currently the Director of the Guangdong Engineering Research Center of Base Station Antennas and Propagation and the Director of the Shenzhen Key Laboratory of Antennas and Propagation. He has authored or coauthored about 200 research articles and books (chapters). He holds about 20 patents. His research interests include wireless communications, antennas, and radio frequency.

Dr. He is a fellow of IET and the Chair of the IEEE Antennas and Propagation Society-Shenzhen Chapter. He was selected as a Pengcheng Scholar Distinguished Professor, Shenzhen. He was a recipient of the Shenzhen Overseas High-Caliber Personnel Level B ("Peacock Plan Award" B) and Shenzhen High-Level Professional Talalent (Local Leading Talent). He received the 2016 Shenzhen Science and Technology Progress Award and the 2017 Guangdong Provincial Science and Technology Progress Award. He is serving as an Associate Editor for IEEE NETWORK, International Journal of Communication Systems, China Communications, and Wireless Communications and Mobile Computing. He served as the General Chair for IEEE ComComAp 2019. He has served as a Reviewer for various journals, such as IEEE TRANSACTIONS ON VEHICULAR TECHNOLOGY, IEEE TRANSACTIONS ON COMMUNICATIONS, IEEE TRANSACTIONS ON WIRELESS COMMUNICATIONS, IEEE TRANSACTIONS ON INDUSTRIAL ELECTRONICS, IEEE TRANSACTIONS ON ANTENNAS AND PROPAGATION, IEEE ANTENNAS AND WIRELESS PROPAGATION LETTERS, IEEE WIRELESS COMMUNICATIONS, IEEE COMMUNICATIONS LETTERS, IEEE JOURNAL ON SELECTED AREAS IN COMMUNICATIONS, *International Journal of Communication Systems, Wireless Communications and Mobile Computing*, and *Wireless Personal Communications*. He has also served as a Technical Program Committee Member or a Session Chair for various conferences, including the IEEE Global Telecommunications Conference (GLOBECOM), the IEEE International Conference on Communications (ICC), the IEEE Wireless Communication Networking Conference (WCNC), the IEEE Vehicular Technology Conference (VTC), the IEEE International Symposium on Antennas and Propagation (APS), the European Conference on Antennas and Propagation (EuCAP), and the Asia-Pacific Microwave Conference (APMC). He is the Principal Investigator for over 30 current or finished research projects, including NSFC of China, the Science and Technology Program of Guangdong Province, as well as the Science and Technology Program of Shenzhen City.

Yadong Yue (Member, IEEE) received the M.S. degree in electronics and communication engineering from Shenzhen University, Shenzhen, China, in 2017.

His research interests include base station antennas and radio frequency.

Long Zhang (Member, IEEE) received the B.S. and M.S. degrees in electrical engineering from the Huazhong University of Science and Technology (HUST), Wuhan, China, in 2009 and 2012, respectively, and the Ph.D. degree in electronic engineering from the University of Kent, Canterbury, U.K, in 2017.

He is currently an Assistant Professor with the College of Electronics and Information Engineering, Shenzhen University, Shenzhen, China. His current research interests include circularly polarized antennas and arrays, millimeter-wave antennas and arrays, phased arrays, tightly coupled arrays, and reflect arrays.

Dr. Zhang served as a Reviewer for several technique journals, including the IEEE TRANSACTIONS ON ANTENNAS AND PROPAGATION, the IEEE ANTENNAS AND WIRELESS PROPAGATION LETTERS, the IET Microwaves, Antennas and Propagation, and Electronic Letters. He was a recipient of the Shenzhen Overseas High-Caliber Personnel Level C ("Peacock Plan Award" C).

Zhi Ning Chen (Fellow, IEEE) received the B.Eng., M.Eng., and Ph.D. degrees in electrical engineering from the Institute of Communications Engineering (ICE), Nanjing, China, in 1985, 1988, and 1993, respectively, and the second Ph.D. degree from the University of Tsukuba, Tsukuba, Japan, in 2003.

From 1988 to 1995, he worked as a Lecturer and later an Associate Professor with ICE and a Post-Doctoral Fellow and later an Associate Professor with Southeast University, Nanjing. From 1995 to 1997, he joined the City University of Hong Kong, Hong Kong, as a Research Assistant and later a Research Fellow. In 1997, he was awarded the Japan Society for the Promotion of Science (JSPS) Fellowship to conduct his research at the University of Tsukuba. From 1999 to 2016, he worked with the Institute for Infocomm Research (I2R), Singapore, as a Principal Scientist, the Head of the RF and Optical Department, and a Technical Advisor. In 2012, he joined the Department of Electrical and Computer Engineering, National University of Singapore, Singapore, as a tenured Full Professor, where he is currently the Program Director (Industry). He is holding/held the concurrent guest professorships at Southeast University (Changjiang Chair Professor); Nanjing University, Nanjing; Tsinghua University, Beijing, China; Shanghai Jiaotong University, Shanghai, China; Tongji University, Shanghai; the University of Science and Technology of China, Hefei, China; Fudan University (Outstanding Visiting Professor), Shanghai; Dalian Maritime University, Dalian, China; Chiba University, Chiba, Japan; the National Taiwan University of Science and Technology, Taipei, Taiwan, Shanghai University (Ziqiang Professor), Shanghai; the Beijing University of Posts and Telecommunications, Tohoku University, Beijing; and the City University of Hong Kong (Adjunct Professor), Hong Kong. He is also serving as the members of State Key Laboratory of Millimeter-waves, Southeast University, and the City University of Hong Kong. He is interested in electromagnetic engineering and antennas/sensors for communication, radar, imaging, and sensing systems. He has published more than 660 academic papers and five books entitled Broadband Planar Antennas (Wiley 2005), UWB Wireless Communication (Wiley 2006), Antennas for Portable Devices (Wiley 2007), Antennas for Base Stations in Wireless Communications (McGraw-Hill 2009), and Handbook of Antenna Technologies with 76 chapters (by Springer References in 2016 as an Editor-in-Chief). He has also contributed the chapters to the books entitled UWB Antennas and Propagation for Communications, Radar, and Imaging (Wiley 2006), Antenna Engineering Handbook (McGraw-Hill 2007), Microstrip and Printed Antennas (Wiley 2010), and Electromagnetics of Body Area Networks (Wiley 2016). He is holding 28 granted/ filed patents with 35 licensed deals with industry.

Dr. Chen was elevated to a fellow of the IEEE for the contribution to small and broadband antennas for wireless applications in 2007. He was elevated to a Fellow of the Academy of Engineering Singapore in 2019. He was a recipient of the International Symposium on Antennas and Propagation Best Paper Award 2010, the CST University Publication Awards 2008 and 2015, the ASEAN Outstanding Engineering Achievement Award in 2013, the Institution of Engineers Singapore Prestigious Engineering Achievement Awards 2006, 2013(2), and 2014, the I2R Quarterly Best Paper Award 2004, the IEEE iWAT 2005 Best Poster Award, several technology achievement awards from China during 1990 to 1997, as well as more than 19 academic awards by the students he supervised. He is the Founding General Chair of the International Workshop on Antenna Technology (iWAT in 2005), the International Symposium on InfoComm and Mechatronics Technology in Bio-Medical and Healthcare Application (IS 3Tin3A in 2010), the International Microwave Forum (IMWF in 2010), and the Asia–Pacific Conference on Antennas and Propagation (APCAP in 2012). He also involved in many international events as the General Chair, the Chair, and a member for technical program committees and international advisory committees. He has served IEEE Council on RFID as a Vice President and a Distinguished Lecturer since 2015. He served on the IEEE TRANSACTION ON ANTENNAS AND PROPAGATION as an Associate Editor and the IEEE Antennas and Propagation Society as a Distinguished Lecturer.